Studies of the edge pedestal and behaviour of Edge Localised Modes in improved H-mode in ASDEX Upgrade

W. Suttrop[1], L. D. Horton[1], C. Konz[1], B. Kurzan[1], C. F. Maggi[1], H. Meister[1], J. Neuhauser[1], A. C. C. Sips[1], H. Urano[2], E. Wolfrum[1], CFN reflectometer group[3] and the ASDEX Upgrade Team

[1]Max-Planck-Institut für Plasmaphysik, EURATOM Association, D-85748 Garching; [2] Japan Atomic Energy Agency, Naka, Ibaraki-ken, 311-0193 Japan; [3]Associação EURATOM/IST, Centro de Fusão Nuclear, Instituto Superior Técnico, 1049-001 Lisboa, Portugal
e-mail: Wolfgang.Suttrop@ipp.mpg.de

Abstract. Improved and conventional high confinement mode discharges in ASDEX Upgrade are compared with respect to H-mode pedestal properties and energy losses due to Edge Localised Modes. In both scenarios, "stiff" temperature profiles and, with few exceptions, only small variations of the density profile shape give rise to a significant correlation between core and pedestal stored energy. The confinement improvement with increased heating power is accompanied with increasing pedestal temperature and pedestal pressure. While the electron temperature barrier width increases with power, the density barrier width remains unchanged or even decreases. The edge pressure gradient increases with power, indicating improved edge stability with increased heating power or beta. The ELM energy loss in improved H-mode is not significantly different from that in conventional H-mode, although there is large scatter in both distributions.

1. Introduction

The 'improved H-mode scenario', studied in ASDEX Upgrade for several years [1], shows high confinement enhancement over H-mode ($H_{98(y,2)} = 1.1 \ldots 1.5$, exceeding the requirements for the ITER H-mode baseline scenario [2]) and is obtained in a wide density range, $\overline{n}_{e,0}/n_{\mathrm{GW}} = 0.3 \ldots 0.9$. Projected to ITER, fusion power comparable with baseline H-mode is achieved with reduced plasma current and higher bootstrap current fraction [3,4]. Because of its potential for long pulse operation (aimed at in advanced scenarios) combined with the robustness of ELMy H-mode, this class of plasmas has also been dubbed the 'hybrid' scenario in studies at JET [5] and DIII-D [6].

In ASDEX Upgrade, improved H-mode is obtained by application of high heating power ($P_{tot} \geq 7.5$ MW) in H-mode discharges with essentially flat central shear profile and central safety factor $q(0) > 1$, i.e. little or no sawteething. Typically, this q profile is achieved by early heating with moderate neutral beam injection (NBI) power during the current rise phase. The slow evolution of the initial q-profile is stabilised by mild central MHD activity, often $m = 1, n = 1$ fishbones or small neoclassical tearing mode islands. Recently, improved confinement with similar q-profile has also been obtained in discharges with late start of NBI heating [7].

To date, the reason for the observed confinement improvement at high heating power is still being investigated. A previous study [8] indicates that the pedestal pressure is higher than in conventional H-mode plasmas. The pedestal pressure plays a role for confinement if "stiff" temperature profiles create a link between the pedestal and core regions, as commonly observed in conventional H-mode plasmas [9]. Compared to conventional H-modes, improved H-mode plasmas show a similar edge-core relationship and similar variation of central density profile peaking, as will be discussed below. The confinement enhancement factor improves with increasing heating power, therefore we examine edge pedestal profiles in heating power scans that have been first presented in Ref. [10], both for early and late heating scenarios. Finally,

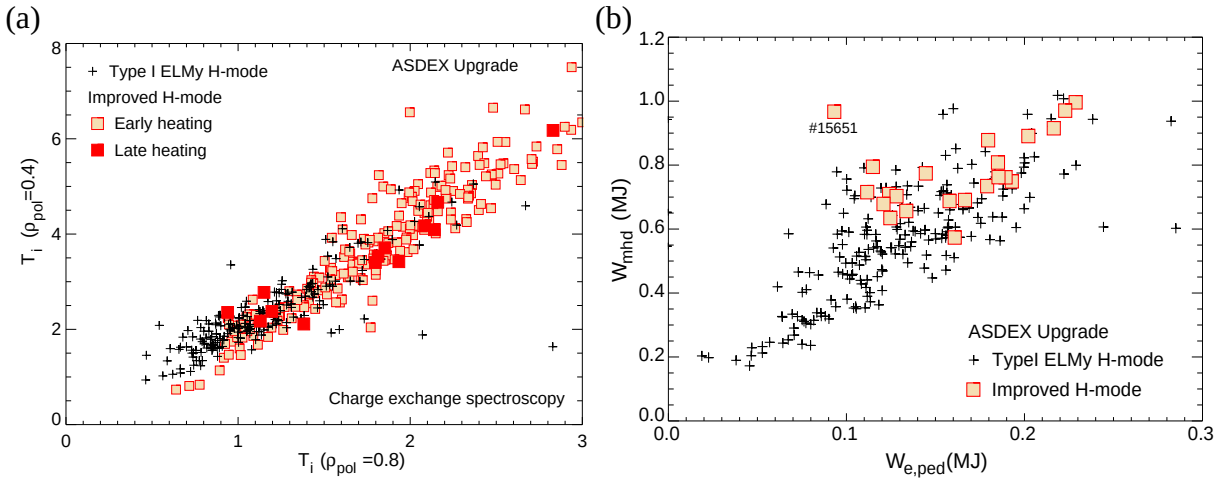

Figure 1: Edge core relation in improved H-mode (squares) and reference type I ELMy H-mode (plus sign) data sets : (a) T_i (at $\rho = 0.4$) vs. (T_i at $\rho = 0.4$), (b) total MHD stored energy vs. pedestal electron energy.

the energy losses associated with Edge Localised Modes (ELMs) are compared between improved and conventional H-mode plasmas. A comparison of the ASDEX Upgrade pedestal measurements to various other tokamaks is presented in Ref. [11].

2. Discharge characterisation

The H-mode discharges considered subsequently are mainly heated by neutral beam injection (NBI), with the addition of centrally deposited ion cyclotron resonance heating (ICRH), which is mostly coupling to the hydrogen minority.
Two main data sets are used:
(a) A comprehensive set of improved H-mode discharges that are performed in ASDEX Upgrade according to the above recipe. This data set is defined in Ref. [3].
(b) As a reference, a selection of longest stationary phases in type I ELMy discharges with largest possible variation of machine parameters. This data set is described in Ref. [12].
Dedicated pedestal profile measurements are only available for subsets of the two data sets. Improved H-mode pedestal data originates from power scans in discharges 20116, 20431 (early heating) and 20448 (late heating), as described in Ref. [10]. Type I ELMy H-mode reference data is taken from the ASDEX Upgrade pedestal data base, which covers a wide parameter range, plasma current $I_p = 0.6 \ldots 1.4$ MA, NBI power $P_{NBI} = 2.5 \ldots 15$ MW, edge safety factor $q_{95} = 3 \ldots 5$ and line-averaged density normalised to the Greenwald limit, $\overline{n}_e / n_{GW} = 0.3 \ldots 0.9$.

2.1. Edge-core relation H-mode plasmas in ASDEX Upgrade show a pronounced relation between edge and core temperatures (both for electrons and ions) [9,13], independent of plasma current, shaping, hydrogen or deuterium, which links the core performance to pedestal top parameters. A linear relationship is found between ion temperatures (T_i) across the confinement region [14]. This relationship is checked in Fig. 1 (a) for improved and reference data sets by plotting $T_i(\rho_p = 0.4)$ vs. $T_i(\rho_p = 0.8)$, where $\rho_p = \overline{\psi}^{1/2}$ and $\overline{\psi}$ the normalised poloidal flux. For improved H-mode with early heating, the same linear relationship between core and peripheral temperature is observed as in the reference data set and as reported in Ref. [14]. Late heating discharges can have weaker core gradients [7]. However, the gradient length $T_i / \nabla T_i$ in improved H-mode is not systematically shorter than in the reference H-mode set, and does not indicate the formation of an internal transport barrier. Inside $\rho_p = 0.4$ there are deviations from

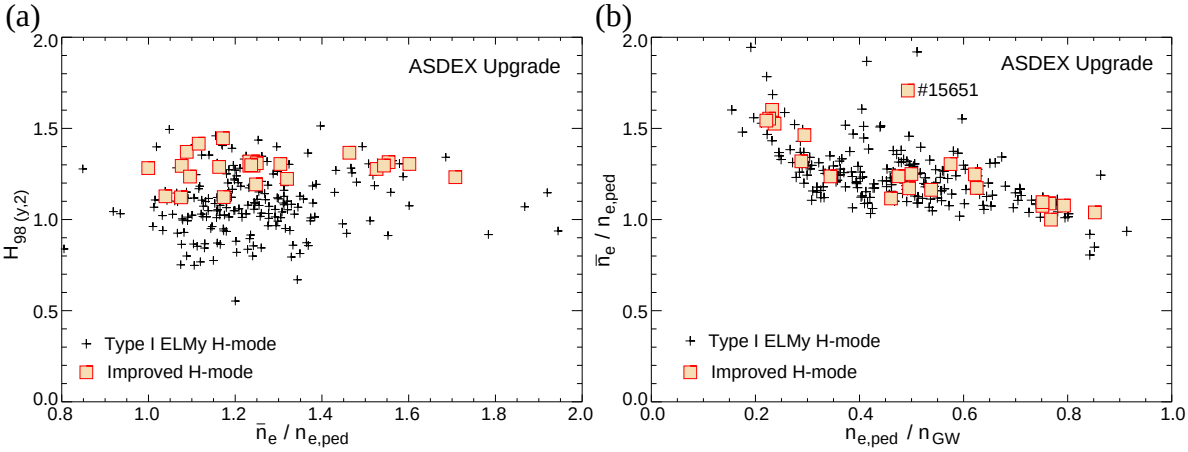

Figure 2: Density peaking: (a) $H_{98(y,2)}$ vs. peaking factor, $\overline{n}_{e,0}/n_e(\rho = 0.9)$, and (b) peaking factor vs. peripheral density $n_e(\rho = 0.9)$ for improved H-mode and standard H-mode plasmas.

proportionality due to presence or absence of sawtooth oscillations, which affect profiles in a small core volume [7].

For similar density profiles, the relation of edge and core temperatures leads to a relationship between total stored energy and pedestal pressure or pedestal energy, which also has been observed in conventional H-modes [15]. Figure 1 (b) shows the MHD stored energy vs. the electron pedestal energy, defined as $(3/2)(k_B\, T_e\, n_e)_{ped} \times V$ (k_B: Boltzmann constant, $T_{e,ped}, n_{e,ped}$: pedestal electron temperature and density, taken here at $\rho_p = 0.9$, V plasma volume) for improved H-mode and reference data sets. Improved H-modes occur at higher values of stored energy, but follow basically the same linear relationship between pedestal and core stored energy as H-modes generally do. As an exception, pulse 15651 (indicated in the figure) shows enhanced stored energy. This is due to a peaked density profile in this discharge (see next section).

2.2. Density peaking Variations of the density profile shape can lead to variations of the relationship between edge pressure and core pressure despite stiff temperature profiles. Confinement improvement with density peaking is found, for example, in completely detached H-mode with radiating mantle [15]. In Fig. 2 (a), $H_{98(y,2)}$ is plotted as a function of $\overline{n}_e/n_e(\rho_p = 0.9)$, which is used here as a measure of density peaking. Improved H-modes populate higher values of the confinement improvement factor, independent of density peaking. The effect of peaked density profiles is mostly contained in the positive line averaged density dependence of the confinement time as predicted by the $H_{98(y,2)}$ scaling. Fig. 2 (b) shows $\overline{n}_e/n_e(\rho_p = 0.9)$ as a function of $n_e(\rho_p = 0.9)/n_{GW}$. With the exception of one pulse, 15651, the density peaking in improved H-mode shows similar behaviour as the reference discharges, i.e. decreasing density peaking with increasing pedestal density.

We conclude that strong density peaking can occur and can lead to improved confinement, as in pulse 15651, but this is not the rule, and in general, improved H-mode confinement in ASDEX Upgrade is not due to peaked density profiles. In fact it is observed that central peaking of the main ion density can cause inward drift of high-Z impurities as predicted for neoclassical transport [16]. In ASDEX Upgrade, with about 90% of the plasma-facing surface covered with tungsten, this inward drift can cause accumulation of tungsten in the core. Operationally, the density peaking is limited by increasing the core heat flux, for example with centrally deposited ICRH, which increases ion diffusivity [17,18]. This technique is regularly applied for improved

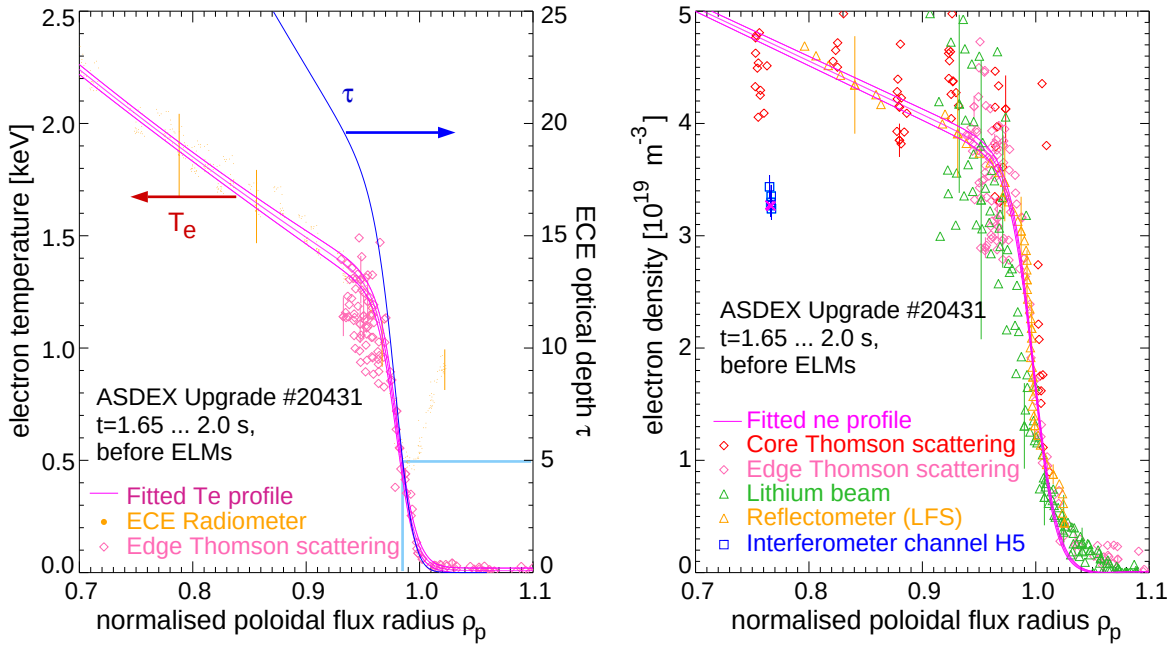

Figure 3: Pedestal profiles of T_e and n_e from various diagnostics with profile fits (see text) and calculated ECE optical depth.

H-mode experiments [19].

3. Edge pedestal measurements

The existence of stiff core profiles and limited variation of the density profile shape suggests that the confinement enhancement in improved H-mode may be due to improved pedestal pressure. In this section, we study the effect of heating power variation on pedestal parameters, in particular the pedestal top temperature and density and the width of the steep gradient region (edge transport barrier).

To assemble high resolution edge profiles, we follow the techniques described in Ref. [20], using electron cyclotron emission (ECE) measurements in the second harmonic X-mode and high resolution edge Thomson scattering [21] for electron temperature profiles, Thomson scattering, microwave reflectometer [22], and Li beam density measurements with ELM resolution [23] for electron density, and charge exchange spectroscopy (CXRS) for ion temperature profiles. Highest resolution edge T_i profiles are obtained by CXRS measurements in the Li-beam [24], however this technique requires extended integration intervals with sufficiently long time intervals in between ELMs which were not obtained in the currently investigated improved H-Mode shots. Hence gradient region width measurements are only presented for electron profiles.

Figure 3 shows examples of T_e and n_e profiles from various diagnostics along with the fitted modified tanh functions [20]. In addition, the ECE second harmonic X-mode optical depth τ is plotted, which is calculated by an approximate formula, $\tau = 3.94 \times T_e n_e$ (keV, 10^{19} m^{-3}) [25]. Only ECE channels with $\tau \geq 5$ are used for the profile fit in order to obtain best radial resolution (close to the width of the cold resonance layer (≈ 5 mm at $B_{RF} = 300$ MHz RF bandwidth) and to avoid overlap of down-shifted ECE from the tail of the energy distribution of electrons located further inside the main plasma. This effect is responsible for the observed signal in channels with cold plasma resonance in the scrape-off-layer. ECE shine-through is commonly observed at the edge of H-mode plasmas and is discussed in detail in Ref. [25].

We investigate the heating power dependence of pedestal parameters in improved H-mode. Fig.

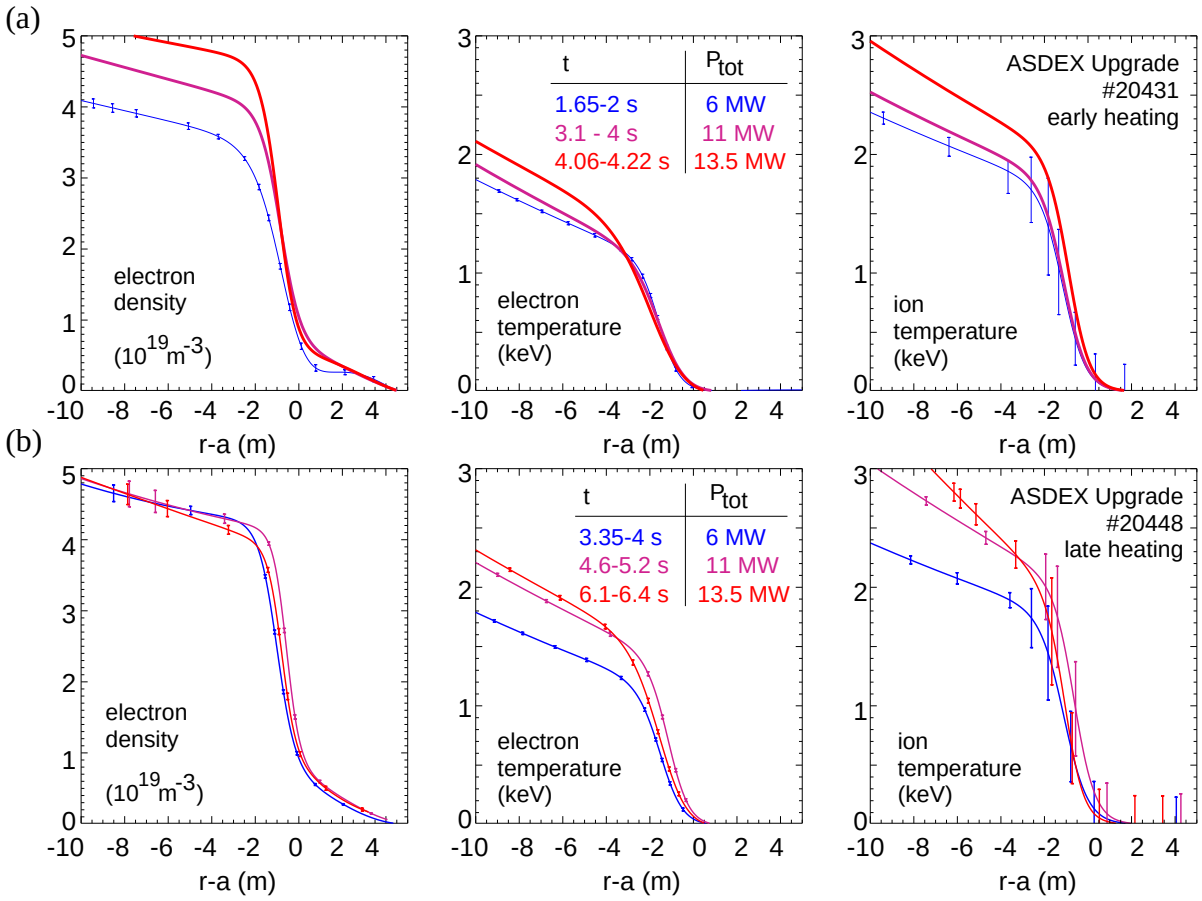

Figure 4: Fitted pedestal profiles for heating power scan (a) with early heating (shot 20431) (b) with late heating (shot 20448)

4 shows the profiles fits of improved H-mode discharges 20431 (late heating) and 20448 (early heating) for various steps of input power, $P_{tot} = 6$, 11 and 13.5 MW. The individual diagnostics profiles are omitted for clarity. The ion temperature profiles are fitted to core CXRS data with barrier width kept fixed at 2 cm.

For early heating (Fig. 4 a) the electron density, electron temperature and ion temperature at the pedestal top all increase with heating power. While the electron density gradient width remains constant or decreases with increasing heating power, the electron temperature width increases keeping the temperature gradient roughly constant. In the case of late heating (Fig. 4 b), the density profile remains unchanged, while both electron and ion temperature at the pedestal top increase with increasing power.

The fit parameters of power scans in three different discharges, 20431 and 20116 (early heating), 20448 (late heating) are summarised in Fig. 5, plotted against the ASDEX Upgrade pedestal data base of type I ELMy discharges for comparison. The pedestal temperature (Fig. 5 a) is highest while the pedestal density (Fig. 5 b) is moderate in the improved H-mode shots under consideration. It must be noted that this is not a restriction; higher density cases exist but are not shown here. The electron temperature and barrier widths (Fig. 5 c and d, respectively) are in the range of those in conventional H-mode, with the marginally significant trend of increasing temperature width and constant or decreasing density width with power. It should be noted that the precision of the edge gradient measurements and the mutual alignment is critical, and the width variations are near the actual resolution of the technique.

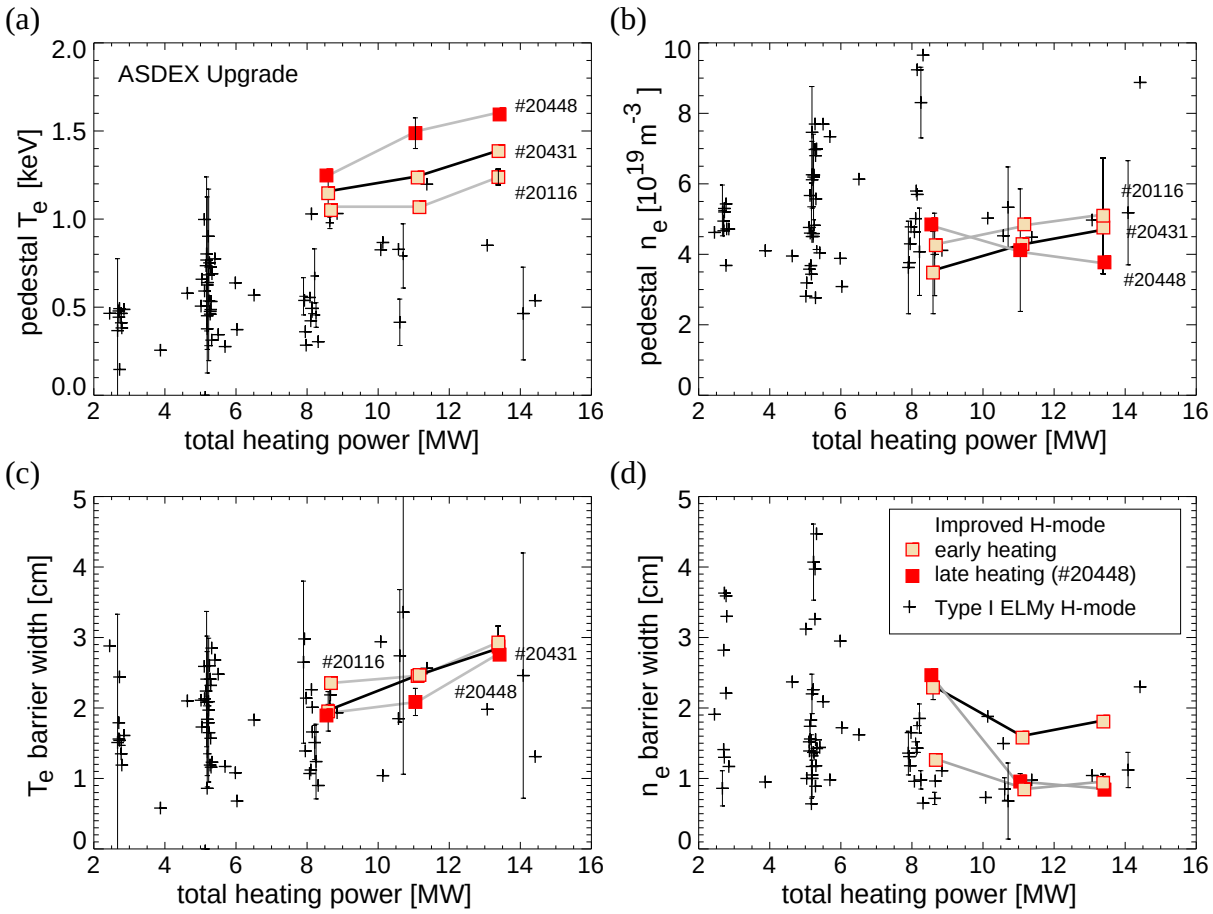

Figure 5: Power dependence of pedestal parameters: (a) pedestal top electron temperature, (b) pedestal top electron density, (c) electron temperature width, (d) electron density width. Data sets are improved H-mode power scans (squares) and H-mode reference (plus signs).

4. ELM energy loss

Subsequently, we discuss whether the confinement improvement in H-mode is systematically connected with larger ELM energy losses. This question is critical, because ELM losses might be large enough in ITER to cause excessive divertor target erosion and tritium co-deposition. The ELM energy loss is evaluated from the change of MHD stored energy before and after an ELM. Fig. 6 shows the ELM energy loss ΔW_{ELM}, normalised to the MHD stored energy W_{MHD}, as a function of various parameters that show significant experimental variation: (a) total heating power P_{tot}, (b) upper triangularity δ_u, (c) pedestal density normalised to the Greenwald density, (d) electron pedestal collisionality $\nu_e^* = \pi R q_{95}/\lambda_{ee}$ (λ_{ee}: mean free path for electron-electron collisions) and (e) edge safety factor q_{95}. The lower triangularity δ_l is strongly correlated with β_p and can therefore not be considered an independent shape parameter. The ELM energy loss shows significant scatter, which has already been noted in Ref. [12]; nevertheless, one can compare standard and improved H-modes. Fig. 6 (a) shows that the upper envelope of observed normalised ELM energy losses decreases with increasing input power. This a consequence of increasing stored energy with heating power; the absolute ELM energy itself does not show a significant variation with input power. A positive q_{95}-dependence can be seen in Fig. 6 (e) for improved H-mode only, which corresponds to a positive B_t dependence in the data. There is no clear dependence on the other three parameters. For lowest ($\delta_u \approx 0$) and highest ($\delta_u > 0.3$) upper

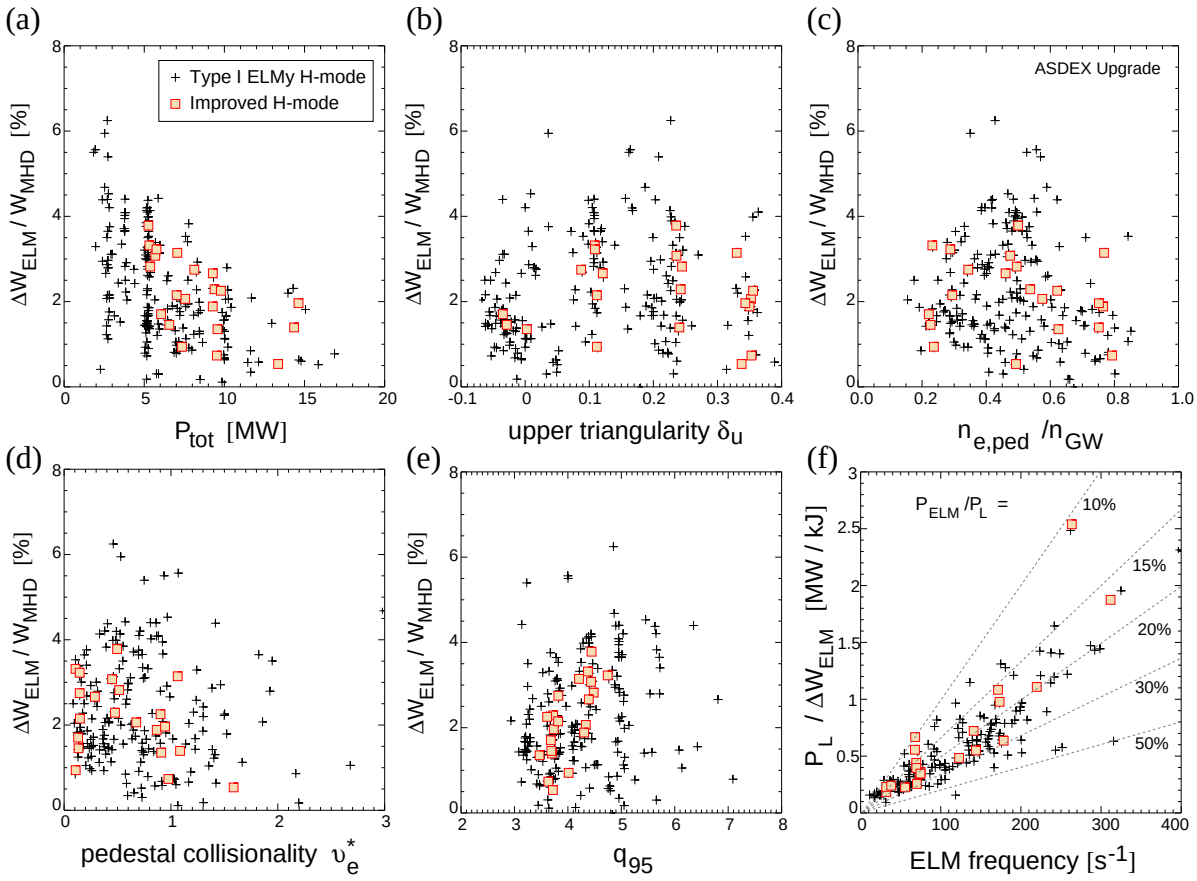

Figure 6: ELM behaviour in improved and standard H-mode discharges: Normalised ELM energy loss $\Delta W_{\mathrm{ELM}}/W_{\mathrm{MHD}}$ as a function of (a) input power, (b) upper triangularity, (c) pedestal Greenwald fraction, (d) electron pedestal collisionality, and (e) edge safety factor q_{95}; (f) $P_{\mathrm{L}}/\Delta W_{\mathrm{ELM}}$ vs. ELM frequency, lines indicate various fractions of power lost during ELMs.

triangularities the normalised ELM energy loss appears to be reduced compared to intermediate δ_u. Finally, Fig. 6 (f) is a plot of $P_L/\Delta W_{\mathrm{ELM}}$ vs. ELM frequency, where P_L is the loss power $P_{tot} - \mathrm{d}W/\mathrm{d}t$. Lines of constant ELM loss power fraction are indicated in the figure. With increasing ELM frequency, the upper bound of ELM loss power fraction seems to decrease from about 50% to 20%. Despite the large scatter in the data, Figs. 6 (a) and (b) indicate that high heating power and high ELM frequency in improved H-mode do not imply larger ELM energy losses than those found in the reference H-mode data set.

5. Summary and Discussion

Power scan experiments in ASDEX Upgrade show that in improved H-mode, the pedestal temperature increases with heating power, which is the main cause for a positive power dependence of the pedestal pressure. Because of stiff core temperature profiles and, in most but not all cases, weak variations of the density profile shape, the increased pedestal pressure accounts at least for part of the observed confinement improvement. Within experimental accuracy, the pedestal temperature increase is connected with a widening of the electron barrier, not an increasing temperature gradient. In Ref. [10], a model is discussed which assumes that the barrier width is determined by the radial region in which the pressure gradient-driven $E \times B$ shearing rate exceeds the ITB growth rate, which depends on the product of toroidal Larmor radius and magnetic shear. The resulting predicted temperature barrier width variation is weak and difficult to test with the present data. In improved H-modes, and unlike most conventional H-modes cases

studied so far, the density barrier width is narrower than the temperature barrier width and, at lowest densities, tends to shrink with heating power. Consequently, the edge pressure gradient remains constant or increases weakly (at low density) with heating power. As discussed in [10], a correlation of β_p with the (electron) pressure gradient exists, which suggests that configuration changes, in particular local magnetic shear and magnetic well can modify edge stability. If the edge radial electrical field E_r is mostly driven by the edge pressure gradient, one would expect only weak variations of E_r in the barrier region. However, Doppler reflectometer measurements in ASDEX Upgrade [26] show that the E_r well depth increases from typically $E_r \approx 30$ keV/m in ELMy H-mode to $E_r \approx 50$ keV/m in improved H-mode, well correlated with the confinement enhancement. The E_r well is always aligned with the steep pressure gradient region. E_r shear can be influential in two ways: (a) weak E_r shear near the pedestal top might reduce ITG turbulence and widen the barrier, and (b) rotational shear along with the E_r shear can enhance MHD stability in the gradient region and steepen the barrier. Whether E_r is mainly driven by the pressure gradient is not clear as yet.

References

[1] GRUBER, O. et al., Phys. Rev. Lett. **83** (1999) 1787.
[2] ITER Physics Expert Groups on Confinement and Modelling and Transport and Confinement Modelling Database et al., Nucl. Fusion **39** (1999) 2175.
[3] SIPS, A. C. C., The performance of improved H-modes at ASDEX Upgrade and projection to ITER, 2006, this conference, EX/1-1.
[4] A.C.C. Sips for the Steady State Operation and the Transport Physics topical groups of the International Tokamak Physics Activity, Plasma Phys. Controlled Fusion **47** (2005) A19.
[5] JOFFRIN, E. et al., The 'hybrid' scenario in JET: Towards its validation for ITER, in *Proc. of the 20th IAEA Conference Fusion Energy (CD-Rom), Vilamoura, Portugal, November 2004*, volume IAEA-CSP-25/CD, pages IAEA–CN–116/4.2, Vienna, 2005, IAEA.
[6] LUCE, T. C. et al., Phys. Plasmas **11** (2004) 2627.
[7] STOBER, J. K., Physics studies of the improved H-mode scenario in ASDEX Upgrade, 2006, this conference, EX/P1-7.
[8] NA, Y.-S. et al., Nucl. Fusion **46** (2006) 232.
[9] STOBER, J. et al., Plasma Phys. Controlled Fusion **42** (2000) A211.
[10] HORTON, L. D. et al., Edge transport barrier characteristics of Improved H-modes in ASDEX Upgrade, 2006, 33rd EPS conference on plasma physics, Rome, P2.140.
[11] MAGGI, C. F., Characteristics of the H-mode pedestal in improved confinement scenarios in ASDEX Upgrade, DIII-D, JET and JT-60U, 2006, this conference, IT/P1-6.
[12] URANO, H. et al., Plasma Phys. Controlled Fusion **45** (2003) 1571.
[13] SUTTROP, W. et al., Plasma Phys. Controlled Fusion **42** (2000) A97.
[14] TARDINI, G. et al., Nucl. Fusion **42** (2002) 258.
[15] SUTTROP, W. et al., Plasma Phys. Controlled Fusion **39** (1997) 2051.
[16] NEU, R. et al., J. Nucl. Mater. **313–316** (2003) 116.
[17] STOBER, J. et al., Nucl. Fusion **41** (2001) 1535.
[18] STOBER, J. et al., Nucl. Fusion **43** (2003) 1265.
[19] STÄBLER, A. et al., Nucl. Fusion **45** (2005) 617.
[20] HORTON, L. D. et al., Nucl. Fusion **45** (2005) 856.
[21] KURZAN, B. et al., Plasma Phys. Controlled Fusion **46** (2004) 299.
[22] MANSO, M. E. et al., Plasma Phys. Controlled Fusion **43** (2001) A73.
[23] BORRASS, K. et al., Nucl. Fusion **40** (2000) 1445.
[24] REICH, M. et al., Plasma Phys. Controlled Fusion **46** (2004) 797.
[25] SUTTROP, W. et al., Practical limitations to plasma edge electron temperature measurements by radiometry of electron cyclotron emission, Technical Report 1/306, IPP, Garching, Germany, 1996.
[26] SCHIRMER, J. et al., Nucl. Fusion **46** (2006) S780.